Very low overhead fault-tolerant magic state preparation using redundant ancilla encoding and flag qubits: Supplementary information

Christopher Chamberland[1,2], Kyungjoo Noh[1]
[1] *AWS Center for Quantum Computing, Pasadena, CA, 91125, USA*
[2] *Institute for Quantum Information and Matter, California Institute of Technology, Pasadena, CA 91125, USA*

SUPPLEMENTARY NOTE 1: GROWING THE TRIANGULAR COLOR CODE

Here, we show how to measure the white plaquettes when implementing the growing schemes in Fig. 7 in the main paper and apply the corrections from the matching graphs results in the correct encoded state. Let us first consider the growing scheme shown in Supplementary Fig. 1a that converts a physical input state $\alpha|0\rangle + \beta|1\rangle$ into a logical state $\alpha|\overline{0}\rangle_{d=5} + \beta|\overline{1}\rangle_{d=5}$ encoded in the distance-5 triangular color code. In this scheme, we first prepare a stabilizer state $|S_t\rangle$ that is stabilized by 14 out of the 18 stabilizer generators of the distance-5 triangular color code

$$g_X^{(3)}, \cdots, g_X^{(9)}, \text{ and } g_Z^{(3)}, \cdots, g_Z^{(9)}, \tag{1}$$

as well as the following four weight-2 stabilizers

$$\begin{aligned} g_X'^{(1)} &= X_3X_5, \quad g_X'^{(2)} = X_{11}X_{15}, \\ g_Z'^{(1)} &= Z_3Z_5, \quad g_Z'^{(2)} = Z_{11}Z_{15}. \end{aligned} \tag{2}$$

We define $\mathcal{S}_{\text{st}}$ to be the group generated by the operators in Eqs. (1) and (2). Note that $|S_t\rangle$ can be prepared by first preparing all qubits in the $|0\rangle$ state, and then measuring only the X-type generators in $\mathcal{S}_{\text{st}}$. As such, we have

$$|S_t\rangle \propto \Big[\prod_{k=1}^{2}(I + g_X'^{(k)})\Big]\Big[\prod_{k=3}^{9}(I + g_X^{(k)})\Big]|0\rangle^{\otimes 18}. \tag{3}$$

One can readily check that $|S_t\rangle$ is stabilized by all the 18 stabilizers in Eqs. (1) and (2) as desired.

Once $|S_t\rangle$ is prepared, we measure the four missing stabilizer generators of the distance-5 triangular code given by

$$\begin{aligned} g_X^{(1)} &= X_1X_2X_3X_4, \quad g_X^{(2)} = X_5X_8X_{11}X_{12}, \\ g_Z^{(1)} &= Z_1Z_2Z_3Z_4, \quad g_Z^{(2)} = Z_5Z_8Z_{11}Z_{12}. \end{aligned} \tag{4}$$

Such operators are the white plaquettes shown in Supplementary Fig. 1a. We define $\mathcal{S}_{b_1}$ to the group generated by the operators in Eq. (4).

Initially, the system is in the state

$$|\psi_0\rangle = (\alpha|0\rangle + \beta|1\rangle) \otimes |S_t\rangle. \tag{5}$$

After measuring the X-type stabilizers of $\mathcal{S}_{b_1}$, we get the following state

$$|\psi_1^{[m_1m_2]}\rangle \propto \prod_{k=1}^{2}(I + (-1)^{m_k} g_X^{(k)})|\psi_0\rangle, \tag{6}$$

conditioned on obtaining $((-1)^{m_1}, (-1)^{m_2})$ where $m_1, m_2 \in \{0,1\}$ when measuring $g_X^{(1)}$ and $g_X^{(2)}$. In any case, we can always convert the state $|\psi_1^{[m_1m_2]}\rangle$ to $|\psi_1^{[00]}\rangle$ by applying a correction operator

$$\begin{cases} I & (m_1,m_2) = (0,0) \\ g_Z'^{(2)} & (m_1,m_2) = (0,1) \\ g_Z'^{(1)} g_Z'^{(2)} & (m_1,m_2) = (1,0) \\ g_Z'^{(1)} & (m_1,m_2) = (1,1) \end{cases} \tag{7}$$

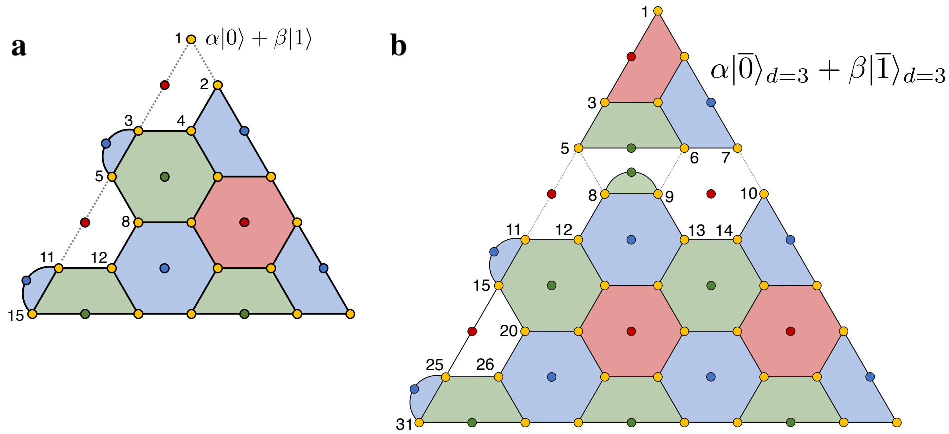

Supplementary Figure 1: Layouts for growing schemes used in the non fault-tolerant preparation of an encoded magic state. **a** An input physical state $\alpha|0\rangle+\beta|1\rangle$ is grown to a logical state $\alpha|\overline{0}\rangle_{d=5}+\beta|\overline{1}\rangle_{d=5}$ encoded in the distance-5 triangular color code. **b** An input logical $\alpha|\overline{0}\rangle_{d=3}+\beta|\overline{1}\rangle_{d=3}$ encoded in the distance-3 triangular color code is grown to a logical state $\alpha|\overline{0}\rangle_{d=7}+\beta|\overline{1}\rangle_{d=7}$ encoded in the distance-7 triangular color code.

since $g_Z'^{(1)}$ anti-commutes with $g_X^{(1)}$ and $g_X^{(2)}$, and $g_Z'^{(2)}$ anti-commutes with $g_X^{(2)}$. Note that the correction operators in Eq. (7) can be determined by implementing MWPM on the matching graph $G_{1x}^{(5)}$ shown in Fig. 7b in the main paper. Thus after the correction, we are always left with the state

$$|\psi_1^{[00]}\rangle \propto \prod_{k=1}^{2}(I+g_X^{(k)})|\psi_0\rangle \propto (\alpha I+\beta X_1)\Big[\prod_{k=1}^{2}(I+g_X'^{(k)})\Big]\Big[\prod_{k=1}^{9}(I+g_X^{(k)})\Big]|0\rangle^{19}, \tag{8}$$

where we used $\alpha|0\rangle+\beta|1\rangle=(\alpha I+\beta X_1)|0\rangle$.

Next, we measure the two Z-type stabilizers of $\mathcal{S}_{b_1}$. After the measurement, the state becomes

$$|\psi_2^{[m_1 m_2]}\rangle \propto \prod_{k=1}^{2}(I+(-1)^{m_k}g_Z^{(k)})|\psi_1^{[00]}\rangle, \tag{9}$$

conditioned on the measurement outcomes $((-1)^{m_1},(-1)^{m_2})$. Performing the same steps as above, the state $|\psi_2^{[m_1 m_2]}\rangle$ can be converted to $|\psi_2^{[00]}\rangle$ by applying an appropriate correction operator which is determined by implementing MWPM on the matching graph $G_{1z}^{(5)}$ shown in Fig. 7b in the main paper. Afterwords, we are left with

$$\begin{aligned}|\psi_2^{[00]}\rangle \propto \prod_{k=1}^{2}(I+g_Z^{(k)})|\psi_1^{[00]}\rangle &\propto \Big[\prod_{k=1}^{2}(I+g_Z^{(k)})\Big](\alpha I+\beta X_1)\Big[\prod_{k=1}^{2}(I+g_X'^{(k)})\Big]\Big[\prod_{k=1}^{9}(I+g_X^{(k)})\Big]|0\rangle^{19}\\ &\propto \Big[\prod_{k=1}^{2}(I+g_Z^{(k)})\Big](\alpha I+\beta X_1)\Big[\prod_{k=1}^{2}(I+g_X'^{(k)})\Big]|\overline{0}\rangle_{d=5}.\end{aligned} \tag{10}$$

where $|\overline{0}\rangle_{d=5}$ is the logical zero state of the distance 5 triangular color code. Note that

$$\begin{aligned}&\Big[\prod_{k=1}^{2}(I+g_Z^{(k)})\Big](\alpha I+\beta X_1)\Big[\prod_{k=1}^{2}(I+g_X'^{(k)})\Big]|\overline{0}\rangle_{d=5}\\ &=\alpha I(I+g_Z^{(1)})(I+g_X'^{(1)})(I+g_Z^{(2)})(I+g_X'^{(2)})|\overline{0}\rangle_{d=5}+\beta X_1(I-g_Z^{(1)})(I+g_X'^{(1)})(I+g_Z^{(2)})(I+g_X'^{(2)})|\overline{0}\rangle_{d=5}\\ &=\alpha I(I+g_Z^{(2)})(I+g_X'^{(2)})(I+g_Z^{(1)})(I+g_X'^{(1)})|\overline{0}\rangle_{d=5}+\beta X_1(I+g_Z^{(2)})(I+g_X'^{(2)})(I-g_Z^{(1)})(I+g_X'^{(1)})|\overline{0}\rangle_{d=5}\\ &\propto \alpha I(I+g_Z^{(2)})(I+g_X'^{(2)})|\overline{0}\rangle_{d=5}+\beta X_1(I+g_Z^{(2)})(I+g_X'^{(2)})g_X'^{(1)}|\overline{0}\rangle_{d=5}\\ &=\alpha I(I+g_Z^{(2)})(I+g_X'^{(2)})|\overline{0}\rangle_{d=5}+\beta X_1 g_X'^{(1)}(I-g_Z^{(2)})(I+g_X'^{(2)})|\overline{0}\rangle_{d=5}\\ &\propto (\alpha I+\beta X_1 g_X'^{(1)}g_X'^{(2)})|\overline{0}\rangle_{d=5}\\ &\propto (\alpha I+\beta X_1X_3X_5X_{11}X_{15})|\overline{0}\rangle_{d=5}.\end{aligned} \tag{11}$$

Since $\overline{X} = X_1X_3X_5X_{11}X_{15}$ is the logical X operator of the distance-5 triangular color code, we can conclude that the output state $|\psi_2^{[00]}\rangle$ is given by

$$|\psi_2^{[00]}\rangle \propto (\alpha I + \beta\overline{X})|\overline{0}\rangle_{d=5} = \alpha|\overline{0}\rangle_{d=5} + \beta|\overline{1}\rangle_{d=5}. \tag{12}$$

Hence, the output state is the desired state $\alpha|\overline{0}\rangle + \beta|\overline{1}\rangle$ encoded in the $d = 5$ triangular color code.

We now move on to the growing scheme shown in Supplementary Fig. 1b that converts an input state $\alpha|\overline{0}\rangle_{d=3} + \beta|\overline{1}\rangle_{d=3}$ (encoded in the $d = 3$ triangular color code) into a logical state $\alpha|\overline{0}\rangle_{d=7} + \beta|\overline{1}\rangle_{d=7}$ encoded in the $d = 7$ triangular color code. As in the previous scheme, we first prepare a stabilizer state $|S_t\rangle$ that is stabilized by 24 out of the 36 generators of the $d = 7$ triangular color code as well as 6 weight-2 stabilizers which are given by

$$\begin{aligned} &g_X'^{(1)} = X_8X_9, \quad g_X'^{(2)} = X_{11}X_{15}, \quad g_X'^{(3)} = X_{25}X_{31}, \\ &g_Z'^{(1)} = Z_8Z_9, \quad g_Z'^{(2)} = Z_{11}Z_{15}, \quad g_Z'^{(3)} = Z_{25}Z_{31}. \end{aligned} \tag{13}$$

To initiate the growing scheme, we measure the following 6 stabilizers of the $d = 7$ triangular color code, which are represented by the white plaquettes of Supplementary Fig. 1b:

$$\begin{aligned} g_X^{(1)} &= X_6X_7X_9X_{10}X_{13}X_{14}, \\ g_X^{(2)} &= X_5X_8X_{11}X_{12}, \quad g_X^{(3)} = X_{15}X_{20}X_{25}X_{26}, \\ g_Z^{(1)} &= Z_6Z_7Z_9Z_{10}Z_{13}Z_{14}, \\ g_Z^{(2)} &= Z_5Z_8Z_{11}Z_{12}, \quad g_Z^{(3)} = Z_{15}Z_{20}Z_{25}Z_{26}. \end{aligned} \tag{14}$$

Note that the operators in Eq. (14) are not stabilizers of the stabilizer state $|S_t\rangle$ and the $d = 3$ triangular color code (which is being merged with $|S_t\rangle$).

Once the stabilizer state is prepared, and prior to measuring the operators in Eq. (14), the system is in the state

$$|\psi_0\rangle = (\alpha|\overline{0}\rangle_{d=3} + \beta|\overline{1}\rangle_{d=3}) \otimes |S_t\rangle. \tag{15}$$

After measuring the three X-type stabilizers in Eq. (14), we get the following state

$$|\psi_1^{[m_1m_2m_3]}\rangle \propto \prod_{k=1}^{3}(I + (-1)^{m_k} g_X^{(k)})|\psi_0\rangle, \tag{16}$$

where the values of $m_1, m_2, m_3 \in \{0, 1\}$ depend on the measurement outcomes of $g_X^{(1)}$, $g_X^{(2)}$ and $g_X^{(3)}$. As in the case where a physical state was grown to an encoded state of the $d = 5$ triangular color code, we can convert any output state $|\psi_1^{[m_1m_2m_3]}\rangle$ to $|\psi_1^{[000]}\rangle$ by applying a correction operator

$$\begin{cases} I & (m_1, m_2, m_3) = (0, 0, 0) \\ g_Z'^{(3)} & (m_1, m_2, m_3) = (0, 0, 1) \\ g_Z'^{(2)} g_Z'^{(3)} & (m_1, m_2, m_3) = (0, 1, 0) \\ g_Z'^{(2)} & (m_1, m_2, m_3) = (0, 1, 1) \\ g_Z'^{(1)} g_Z'^{(2)} g_Z'^{(3)} & (m_1, m_2, m_3) = (1, 0, 0) \\ g_Z'^{(1)} g_Z'^{(2)} & (m_1, m_2, m_3) = (1, 0, 1) \\ g_Z'^{(1)} & (m_1, m_2, m_3) = (1, 1, 0) \\ g_Z'^{(1)} g_Z'^{(3)} & (m_1, m_2, m_3) = (1, 1, 1) \end{cases}. \tag{17}$$

Note that correction operators of Eq. (17) can be determined by implementing MWPM on the matching graph $G_{3x}^{(7)}$ shown in Fig. 7d in the main paper. After the applying such corrections, we are always left with the state

$$|\psi_1^{[000]}\rangle \propto \prod_{k=1}^{3}(I + g_X^{(k)})|\psi_0\rangle. \tag{18}$$

The final step consists of measuring the three Z-type stabilizers in Eq. (14). The state in Eq. (18) then becomes

$$|\psi_2^{[m_1 m_2 m_3]}\rangle \propto \prod_{k=1}^{3} (I + (-1)^{m_k} g_Z^{(k)}) |\psi_1^{[000]}\rangle, \tag{19}$$

where the values of $m_1, m_2, m_3 \in \{0, 1\}$ depend on the measurement outcomes of $g_Z^{(1)}$, $g_Z^{(2)}$ and $g_Z^{(3)}$. The states $|\psi_2^{[m_1 m_2 m_3]}\rangle$ can be mapped to the state $|\psi_2^{[000]}\rangle$ again by applying an appropriate correction operator as was done in Eq. (17), but with X-type operators. Thus, at the end of the growing scheme, we have

$$|\psi_2^{[000]}\rangle \propto \Big[\prod_{k=1}^{3} (I + g_Z^{(k)})\Big] |\psi_1^{[000]}\rangle \propto \Big[\prod_{k=1}^{3} (I + g_Z^{(k)})\Big]\Big[\prod_{k=1}^{3} (I + g_X^{(k)})\Big] |\psi_0\rangle. \tag{20}$$

Repeating a similar analysis as in Eq. (11), we get the following desired result

$$|\psi_2^{[000]}\rangle \propto \alpha|\overline{0}\rangle_{d=7} + \beta|\overline{1}\rangle_{d=7}. \tag{21}$$

SUPPLEMENTARY NOTE 2: PROOF OF THE FAULT-TOLERANCE OF OUR MAGIC STATE PREPARATION SCHEME

Here, we show that in order for the magic state preparation protocol of Fig. 1 in the main paper to be fault-tolerant (see Definition 2 in the main paper), the pair of $H_m^{(d)}$ and $EC^{(d)}$ circuits need to be repeated a minimum of $(d-1)/2$ times. Note that we have verified numerically that the $H_m^{(d)}$ and $EC^{(d)}$ circuits are t-flag circuits (with $t = (d-1)/2$). Hence if there are $s \leq t$ faults in the $H_m^{(d)}$ or $EC^{(d)}$ circuits resulting in an error E with either $\min(\mathrm{wt}(E), \mathrm{wt}(E\overline{H})) > s$ or $\min(\mathrm{wt}(E), \mathrm{wt}(EP)) > s$ (for any of the stabilizers P), at least one flag qubit will flag and the protocol aborts.

First, we consider all the possible output errors of the fault-free implementation of the $H_m^{(d)}$ circuits given an input error E_{in} (see Supplementary Fig. 2). The input error E_{in} arises from faults which occur during the implementation of the $G^{(1\to d)}$ circuit (see for instance Fig. 7 in the main paper or Supplementary Fig. 1). We illustrate all possible cases for E_{in} and for each case we show the resulting output errors. Note that in what follows, the state $|\mathrm{GHZ}\rangle = \frac{1}{\sqrt{2}}(|0\rangle^{\otimes m} + |1\rangle^{\otimes m})$ (where m is the number of ancilla qubits) can be replaced by the single-qubit $|+\rangle$ state without changing the final result. We also write the controlled-Hadamard gate as $C_{\overline{H}}$. Lastly, given an error E, $s(E)$ will correspond to the error syndrome of E obtained by measuring all the stabilizer generators of the underlying stabilizer code used to encode the data.

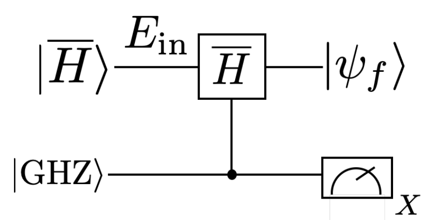

Supplementary Figure 2: Schematic for the implementation of the $H_m^{(d)}$ circuit with an input error E_{in}, resulting in an output state $|\psi_f\rangle$. A GHZ state is prepared and the parity of the logical Hadamard operator $\overline{H} = H^{\otimes n}$ is measured. We omit the details for the fault-tolerant preparation of the GHZ state (see for instance Fig. 3 in the main paper) as it is not important for the discussion in this section.

Case 1: $E_{\mathrm{in}} = \overline{X}$ or $E_{\mathrm{in}} = \overline{Z}$. Suppose $E_{\mathrm{in}} = \overline{X}$. Prior to performing the $C_{\overline{H}}$ gate, we have

$$|\psi_1\rangle = \overline{X}|\overline{H}\rangle \otimes |+\rangle = \frac{1}{\sqrt{2}}(\overline{X}|\overline{H}\rangle \otimes |0\rangle + \overline{X}|\overline{H}\rangle \otimes |1\rangle). \tag{22}$$

Applying the $C_{\overline{H}}$ gate and using the identity $HX = ZH$, $|\psi_1\rangle$ transforms to $|\psi_2\rangle$ which is given by

$$\begin{aligned} |\psi_2\rangle = \frac{1}{\sqrt{2}}(\overline{X}|\overline{H}\rangle \otimes |0\rangle + \overline{Z}|\overline{H}\rangle \otimes |1\rangle) &= \frac{1}{\sqrt{2}}(\frac{\overline{X}+\overline{Z}}{\sqrt{2}}|\overline{H}\rangle \otimes |+\rangle + \frac{\overline{X}-\overline{Z}}{\sqrt{2}}|\overline{H}\rangle \otimes |-\rangle) \\ &= \frac{1}{\sqrt{2}}(|\overline{H}\rangle \otimes |+\rangle + \frac{\overline{X}-\overline{Z}}{\sqrt{2}}|\overline{H}\rangle \otimes |-\rangle). \end{aligned} \tag{23}$$

Similarly, if $E_{\text{in}} = \overline{Z}$, performing the same steps shows that

$$|\psi_2\rangle = \frac{1}{\sqrt{2}}(|\overline{H}\rangle \otimes |+\rangle - \frac{\overline{X}-\overline{Z}}{\sqrt{2}}|\overline{H}\rangle \otimes |-\rangle). \tag{24}$$

From Eqs. (23) and (24), we see that performing the X-basis measurement and discarding the ancilla, the final output state $|\psi_3\rangle$ is $|\psi_f\rangle = |\overline{H}\rangle$ if a $+1$ outcome is obtained (which is the desired state), and $|\psi_f\rangle = \frac{\overline{X}-\overline{Z}}{\sqrt{2}}|\overline{H}\rangle$ if a -1 outcome is obtained (each occurring with a 50% probability).

Case 2: $E_{\text{in}} = \overline{Y}$. Prior to performing the $C_{\overline{H}}$ gate, we have

$$|\psi_1\rangle = \overline{Y}|\overline{H}\rangle \otimes |+\rangle = \frac{1}{\sqrt{2}}(\overline{Y}|\overline{H}\rangle \otimes |0\rangle + \overline{Y}|\overline{H}\rangle \otimes |1\rangle). \tag{25}$$

Applying the $C_{\overline{H}}$ gate and using the identity $HY = -YH$, we have

$$|\psi_2\rangle = \frac{1}{\sqrt{2}}(\overline{Y}|\overline{H}\rangle \otimes |0\rangle - \overline{Y}|\overline{H}\rangle \otimes |1\rangle) = \overline{Y}|\overline{H}\rangle \otimes |-\rangle. \tag{26}$$

Hence the ancilla measurement outcome will always be -1 with the final output state $|\psi_f\rangle = \overline{Y}|\overline{H}\rangle$.

Case 3: $E_{\text{in}} = E'\overline{Y}$. In this case, we assume that $s(E') \neq \mathbf{0}$ where $\mathbf{0}$ is the all zeros bit string of length $n-1$ (where n is the number of data qubits of the underlying stabilizer code encoding the data). Further, we define $\tilde{E}' = \overline{H}E'\overline{H}^\dagger$. Performing an analogous calculation to the one leading to Eq. (26), we have

$$|\psi_2\rangle = \frac{1}{\sqrt{2}}(\frac{(E'-\tilde{E}')}{\sqrt{2}}\overline{Y}|\overline{H}\rangle \otimes |+\rangle + \frac{(E'+\tilde{E}')}{\sqrt{2}}\overline{Y}|\overline{H}\rangle \otimes |-\rangle). \tag{27}$$

Hence, if the ancilla is measured as $+1$, the output state will be $|\psi_f\rangle = \frac{(E'-\tilde{E}')}{\sqrt{2}}\overline{Y}|\overline{H}\rangle$ whereas a -1 outcome will yield $|\psi_f\rangle = \frac{(E'+\tilde{E}')}{\sqrt{2}}\overline{Y}|\overline{H}\rangle$. Both measurement outcomes occur with 50% probability. Further, note that $\frac{(E'-\tilde{E}')}{\sqrt{2}}$ and $\frac{(E'+\tilde{E}')}{\sqrt{2}}$ are detectable errors.

Case 4: $E_{\text{in}} = E'\overline{X}$ or $E_{\text{in}} = E'\overline{Z}$. Again, we assume that $s(E') \neq \mathbf{0}$. Performing the same calculations as above, we find

$$|\psi_2\rangle = \frac{1}{\sqrt{2}}(\frac{(E'\overline{X}+\tilde{E}'\overline{Z})}{\sqrt{2}}|\overline{H}\rangle \otimes |+\rangle + \frac{(E'\overline{X}-\tilde{E}'\overline{Z})}{\sqrt{2}}|\overline{H}\rangle \otimes |-\rangle). \tag{28}$$

Again, the ancilla measurement outcomes will be ± 1, each occurring with 50% probability. A $+1$ outcome yields the output state $|\psi_f\rangle = \frac{(E'\overline{X}+\tilde{E}'\overline{Z})}{\sqrt{2}}|\overline{H}\rangle$ and a -1 outcome yields $|\psi_f\rangle = \frac{(E'\overline{X}-\tilde{E}'\overline{Z})}{\sqrt{2}}|\overline{H}\rangle$. In both cases, the errors afflicting the state $|\overline{H}\rangle$ will be detected by a fault-free $EC^{(d)}$ circuit. The case where $E_{\text{in}} = E'\overline{Z}$ yields identical output states, up to a global sign. We will now explain why the $H_m^{(d)}$ and $EC^{(d)}$ circuits need to come in pairs.

In the example provided leading to Eq. (28), if the $+1$ measurement outcome is obtained, there can be a fault resulting in the error E' at the very beginning of the subsequent $EC^{(d)}$ circuit cancelling the term multiplying $\overline{X}$ and thus resulting in the error $E = \frac{\overline{X}+E'\tilde{E}'\overline{Z}}{\sqrt{2}}$. As such, there is a 50% chance that a trivial syndrome is obtained when implementing the $EC^{(d)}$ circuit, resulting in the output error $\overline{X}$. However, by applying the $H_m^{(d)}$ circuit a second time (assuming it is fault-free), Case 1 shows that a $+1$ outcome cannot result in an output state with a logical fault. Since the pair of $H_m^{(d)}$ and $EC^{(d)}$ circuits are repeated $(d-1)/2$ times, at least one such pair must be fault-free if the total number of faults v has $v \leq (d-1)/2$. This example illustrates the importance of applying the $H_m^{(d)}$ and $EC^{(d)}$ circuits in pairs. For instance, if all the $H_m^{(d)}$ circuits were repeated $(d-1)/2$ times, followed by the repetition of the $EC^{(d)}$ circuits $(d-1)/2$ times, an error of the form $\frac{(E'\overline{X}+\tilde{E}'\overline{Z})}{\sqrt{2}}$ would always result in a $+1$ outcome of the $H_m^{(d)}$ circuits and the output error would be unchanged. Then as shown above, a single fault at the beginning of the first $EC^{(d)}$ circuit could result in a trivial syndrome with 50% probability (with an output error $\overline{X}$) and all subsequent rounds of syndrome measurement would yield the trivial syndrome.

Now suppose there are $s = (d-1)/2$ faults spread throughout all the circuits illustrated in Fig. 1 in the main paper. We consider the worst case scenario, where a single fault results in an error E (which should be detected by our protocol), and the remaining $s-1$ faults all result in measurement errors (and such faults can potentially add additional data qubit errors, say if it arises from a CNOT gate) preventing E from being detected in either the $H_m^{(d)}$ or $EC^{(d)}$ circuits. Since the pair of $H_m^{(d)}$ and $EC^{(d)}$ circuits are repeated $(d-1)/2$ times, at least one pair of $H_m^{(d)}$ and $EC^{(d)}$ circuits will be fault-free and thus not afflicted by measurement errors. From the above, if the $H_m^{(d)}$ and $EC^{(d)}$ circuits are fault-free, then $+1$ measurement outcomes in both circuits cannot yield an uncorrectable output error. Further, since all the $H_m^{(d)}$ and $EC^{(d)}$ circuits are t-flag circuits (with $t=(d-1)/2$), the final output error E_{final} must have $\text{wt}(E_{\text{final}})\leq s$ and as such, it must be a correctable error.

We note that in the general case, where a $|\text{GHZ}\rangle$ state is used instead of the $|+\rangle$ state, we can replace $+1$ and -1 measurement outcomes with even and odd parity measurement outcomes, and the same conclusions would follow.

SUPPLEMENTARY NOTE 3: TWIRLING APPROXIMATION

Here, we show that a non-Pauli error after a $T^\dagger$ or T gate can be converted via a noise twirling operation into an incoherent mixture of Pauli errors. To be clear, we do not propose to physically perform the noise twirling after the $T^\dagger$ and T gates as part of the protocol as this can reduce the performance of our scheme. Instead, we aim to show that the approximations we performed in our numerical simulations are justified.

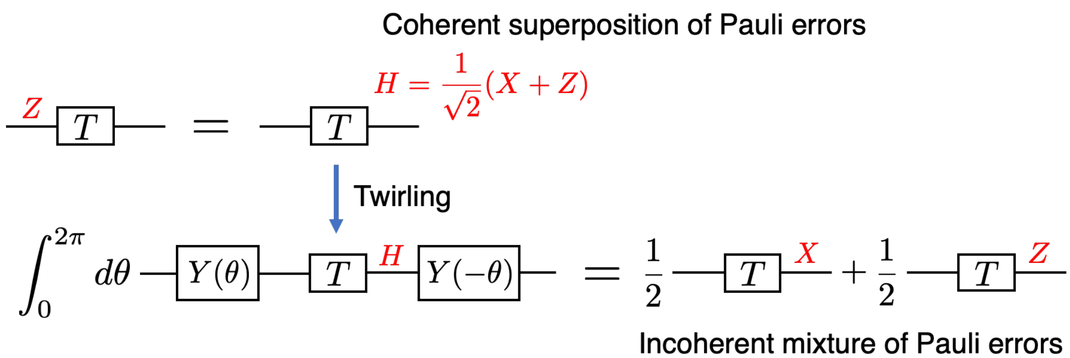

Supplementary Figure 3: Conversion of a Hadamard error $H=(X+Z)/\sqrt{2}$ (i.e., coherent superposition of Pauli errors) into an incoherent mixture of Pauli errors X and Z via a noise twirling. Note that $Y(\theta)$ is defined as $Y(\theta)\equiv\exp[-i(\theta/2)Y]$ and $T=Y(\pi/4)$.

Suppose for instance there is an input Z error to a T gate. Recall that the input Pauli error Z is converted through the T gate into a non-Pauli error $H=\frac{1}{\sqrt{2}}(X+Z)$. We make this non-Pauli error into an incoherent mixture of Pauli errors by applying $Y(\theta)$ and $Y(-\theta)$ before and after the noisy T gate where the rotation angle θ is drawn uniformly from the range $[0,2\pi]$. Note that

$$\rho'\equiv\int_0^{2\pi}d\theta Y(-\theta)HTY(\theta)\rho Y(-\theta)T^\dagger HY(\theta)=\int_0^{2\pi}d\theta Y(-\theta)HY(\theta)(T\hat{\rho}T^\dagger)Y(-\theta)HY(\theta), \tag{29}$$

where we used the fact that $T=Y(\frac{\pi}{4})$ commutes with $Y(\theta)$ for any $\theta\in[0,2\pi]$. Then, since

$$\begin{aligned} Y(-\theta)XY(\theta)&=\cos\theta X+\sin\theta Z,\\ Y(-\theta)ZY(\theta)&=-\sin\theta X+\cos\theta Z, \end{aligned} \tag{30}$$

we have

$$Y(-\theta)HY(\theta)=\frac{1}{\sqrt{2}}Y(-\theta)(X+Z)Y(\theta)=\cos\left(\theta+\frac{\pi}{4}\right)X+\sin\left(\theta+\frac{\pi}{4}\right)Z, \tag{31}$$

and thus

$$\begin{aligned} \rho'&=\int_0^{2\pi}d\theta\Big[\cos^2\left(\theta+\frac{\pi}{4}\right)X(T\rho T^\dagger)X+\sin^2\left(\theta+\frac{\pi}{4}\right)Z(T\rho T^\dagger)Z\\ &\qquad+\frac{1}{2}\sin\left(2\theta+\frac{\pi}{2}\right)X(T\rho T^\dagger)Z+\frac{1}{2}\sin\left(2\theta+\frac{\pi}{2}\right)Z(T\rho T^\dagger)X\Big]\\ &=\frac{1}{2}\Big[X(T\rho T^\dagger)X+Z(T\rho T^\dagger)Z\Big]. \end{aligned} \tag{32}$$

That is, the output Hadamard error $H = \frac{1}{\sqrt{2}}(X + Z)$ is converted via the noise twirling to an incoherent mixture of the Pauli X and Z errors, each with 50% probability (see Supplementary Fig. 3). The same reasoning holds for any output error $\cos\phi X + \sin\phi Z$ for any $\phi \in [0, 2\pi]$. On the other hand, since a Pauli Y error commutes with the T gate and the $Y(\theta)$ gates, it is unaffected by the noise twirling and remains to be a Pauli Y error.

SUPPLEMENTARY NOTE 4: PREPARING AN H-TYPE MAGIC STATE WITH PHYSICAL STABILIZER OPERATIONS

Here, we discuss more details on the simulation of non-Clifford gates. Note that an X error propagating through the control qubit of a controlled-Hadamard gate results in a Hadamard error applied to the data (see Supplementary Fig. 4). Therefore, an $X \otimes X$ error on the first CNOT between the ancillas $|+\rangle$ and $|0\rangle$ in the circuit implementing $H_m^{(d)}$ results in the error $H^{\otimes n}$ (which acts trivially on $|\overline{H}\rangle$) without any flag qubits flagging (see Supplementary Fig. 5 for an illustration). However, since the controlled-Hadamard is decomposed as in Fig. 5b in the main paper, an X error on the control qubit of the controlled-Z gate results in a Z error on the data. Therefore, if we propagate $Z^{\otimes n}$ (arising from the $X \otimes X$ error at the CNOT mentioned above) through the T gates as described above, the output will not be a benign error. As such, prior to the application of the T gates, let E_Z be the Z component of the data qubit errors. For instance, if the data qubit errors are $E = Z \otimes X \otimes Y$, then $E_Z = Z \otimes I \otimes Z$. The Z component which is propagated through the T gates is chosen to be $E'_Z = \min(\text{wt}(E_Z), \text{wt}(E_Z Z^{\otimes n}))$. This prevents a single fault from causing a logical error without any flag qubits flagging in our simulations.

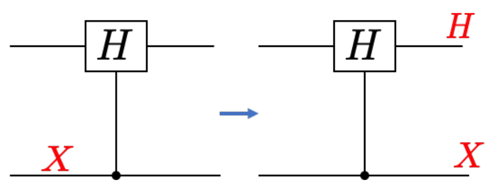

Supplementary Figure 4: An X error on the control qubit of the controlled-Hadamard gate results in an H error on the target qubit.

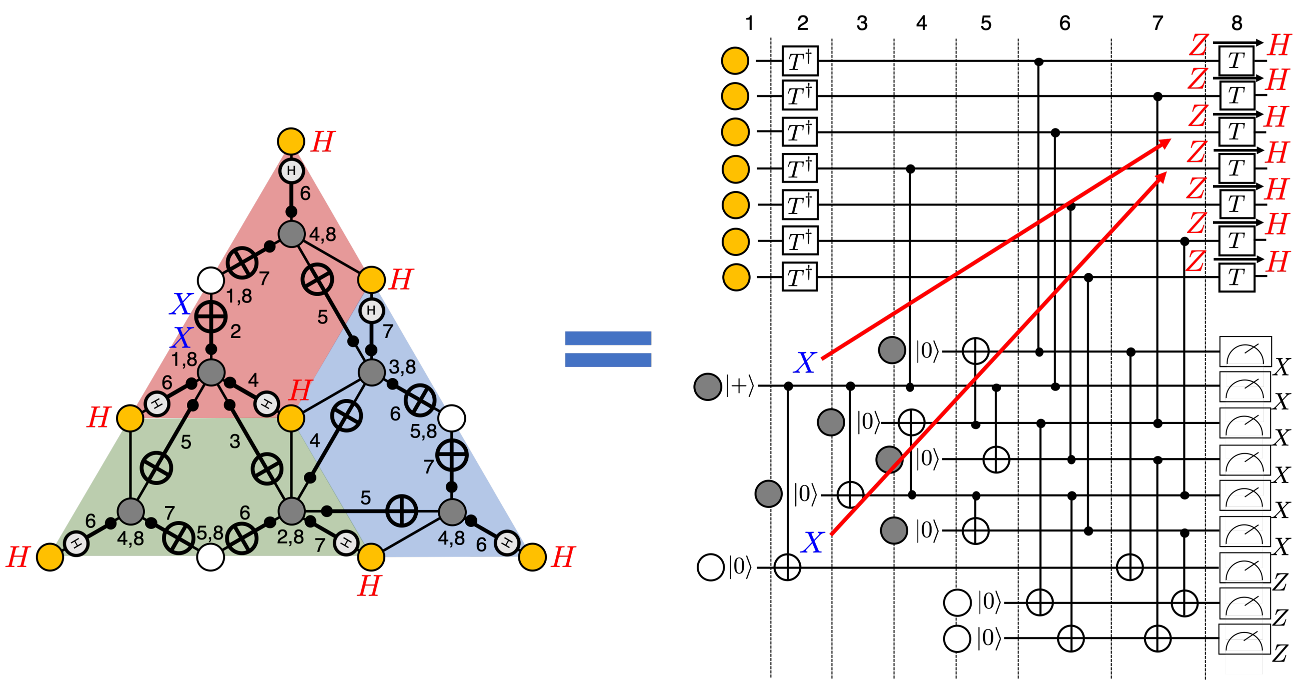

Supplementary Figure 5: Example of an $X \otimes X$ error on a CNOT gate of the circuit $H_m^{(3)}$ resulting in a $\overline{H} = H^{\otimes n}$ data qubit error without any flag qubits flagging. However, such an error acts trivially on the $|\overline{H}\rangle$ state being prepared.

SUPPLEMENTARY NOTE 5: PREPARING AN H-TYPE MAGIC STATE WITH ENCODED STABILIZER OPERATIONS

Here, we provide a detailed overhead analysis of our magic state preparation scheme with stabilizer operations encoded in the triangular color code.

Recall that to prepare an $|\overline{H}\rangle_f$ state with some target logical error rate, we require all stabilizer operations to be encoded in a triangular color code of distance d_2. First, $|\overline{H}\rangle_{d_1}$ states are prepared using the scheme described in Fig. 1 in the main paper (with $d_1 \in \{3, 5, 7\}$ and with physical stabilizer operations). The distance d_1 is chosen such that the $|\overline{H}\rangle_{d_1}$ states have smaller logical failure rates compared with those of the distance d_2 encoded stabilizer operations. The $|\overline{H}\rangle_{d_1}$ states are used to implement the logical T gates (see Fig. 5a in the main paper) and for injection in the circuit $\tilde{G}^{(1\rightarrow d_f)}$. If $d_1 < d_2$, the $|\overline{H}\rangle_{d_1}$ states must first be grown into $|\overline{H}\rangle_{d_2}$ states using the growing circuit $G^{(d_1\rightarrow d_2)}$ shown in Fig. 7c in the main paper or in Supplementary Fig. 1b. Note that we did not put the tilde on $G^{(d_1\rightarrow d_2)}$ since all operations are implemented with physical gates. Using encoded $|\overline{H}\rangle_{d_2}$ states ensures that stabilizer operations encoded in a distance d_2 triangular color code can be used with the prepared magic states.

Once enough $|\overline{H}\rangle_{d_2}$ states have been prepared (see below), such states are injected into the circuits of Fig. 5a in the main paper to perform the logical T gates, in addition to being injected in the circuit $\tilde{G}^{(1\rightarrow d)}$ (see for instance the circuit used in Fig. 7a in the main paper or Supplementary Fig. 1a, but with distance d_2 encoded stabilizer operations). The final $|\overline{H}\rangle_f$ state used for computation is then prepared repeating the same steps as in Fig. 1 in the main paper (i.e. applying $(d_f - 1)/2$ pairs of the $\tilde{H}_m^{(d)}$ and $\tilde{EC}^{(d)}$ circuits) with each stabilizer operation encoded in the distance d_2 triangular color code. In Supplementary Fig. 6 we provide a schematic illustration of the full scheme described above.

To compute the overhead for preparing the state $|\overline{H}\rangle_f$, we consider the case where all the $T^\dagger$ gates are simultaneously

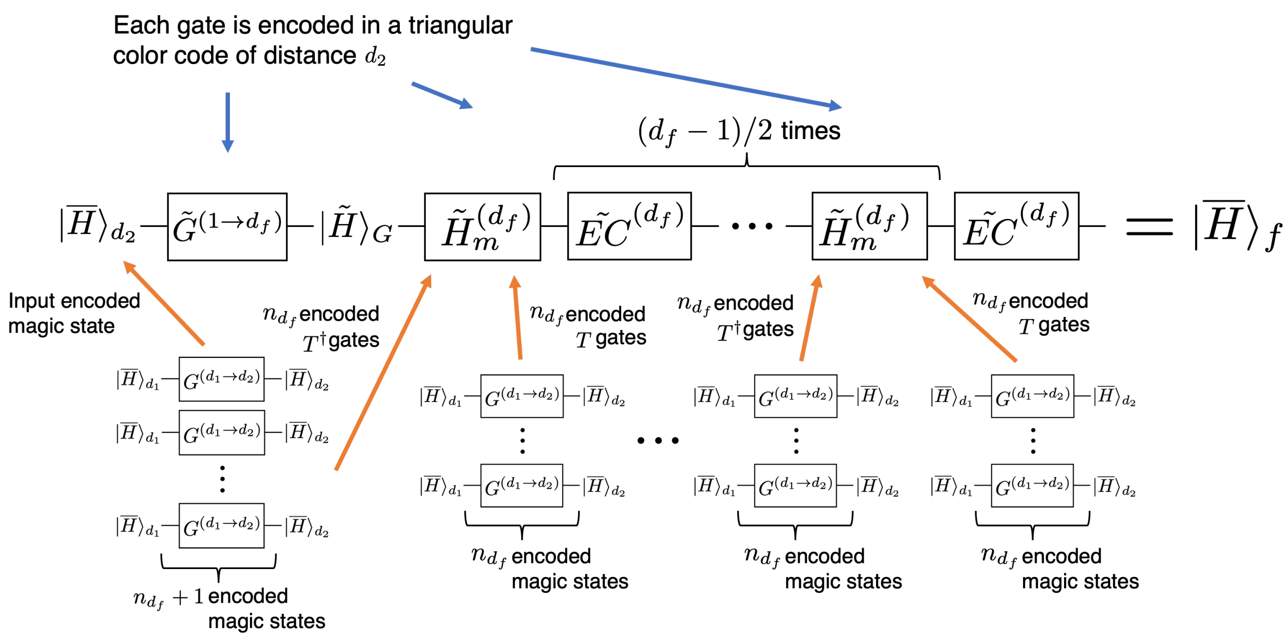

Supplementary Figure 6: General scheme for fault-tolerantly preparing an encoded magic state. Unlike in Fig. 1 in the main paper, each gate is encoded in a triangular color code of distance d_2. Magic states that are encoded in a triangular color code of distance d_1 (i.e., $|\overline{H}\rangle_{d_1}$) are directly prepared by using the scheme in Fig. 1 in the main paper. These magic states are then grown to the distance d_2 triangular color code (i.e., $|\overline{H}\rangle_{d_2}$) by using the growing scheme in Fig. 7c in the main paper or in Supplementary Fig. 1b. Initially, $m_{d_f} \geq n_{d_f} + 1$ encoded magic states $|\overline{H}\rangle_{d_2}$ are prepared where $n_{d_f} \equiv (3d_f^2 + 1)/4$ (see Eq. (33) for the definition of m_{d_f}). One of these encoded magic states is further grown to $|\tilde{H}\rangle$ via a growing circuit $\tilde{G}^{1\rightarrow d_f}$ where each gate is encoded in the distance d_2 color code. The remaining n_{d_f} encoded magic states are used to implement the n_{d_f} encoded $T^\dagger$ gates in the $\tilde{H}_m^{(d_f)}$ circuit. While the circuit $\tilde{H}_m^{(d_f)}$ is being implemented, another n_{d_f} encoded magic states need to be prepared so that they can be used to implement n_{d_f} encoded T gates at the end of the $\tilde{H}_m^{(d_f)}$ circuit. Since the circuit $\tilde{H}_m^{(d_f)}$ is repeated $(d_f - 1)/2$ times, we need in total $(d_f - 1)n_{d_f} + 1$ encoded magic states $|\overline{H}\rangle_{d_2}$. The $\tilde{EC}^{(d_f)}$ circuits are used to measure the stabilizers of the triangular color codes but with encoded d_2 stabilizer operations.

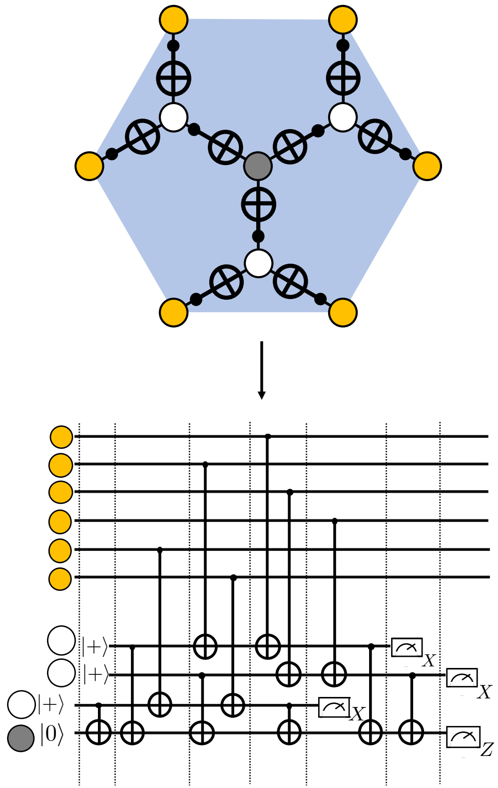

Supplementary Figure 7: Weight-six Z-type stabilizer plaquette used in the lattice $\mathcal{L}$ for performing the encoded Clifford operations. The plaquettes used for preparing the stabilizer state $|S_t\rangle$ which is gauge fixed with $|\overline{H}\rangle_{d_1}$ also use the layout shown in this figure. The X-type stabilizer is obtained by inverting the directions of the CNOT gates, swapping $|0\rangle$ with $|+\rangle$ and exchanging the Z-basis measurements with X-basis measurements.

implemented during the second time step of the $H_m^{(d)}$ circuit. We can thus prepare m_{d_f} $|\overline{H}\rangle_{d_1}$ states which are used for implementing the $T^\dagger$ gates in addition to injecting one of these states into the circuit $\tilde{G}^{(1\rightarrow d)}$. The probability that at least $(3d_f^2+1)/4+1 = n_{d_f}+1$ $|\overline{H}\rangle_{d_1}$ states pass the verification test is given by

$$P_{A,d_f}^{(n_{d_f})}(p, m_{d_f}) = \sum_{k=n_{d_f}+1}^{m_{d_f}} \binom{m_{d_f}}{k} p_{\text{acc}}^{(d_1)}(p)(1-p_{\text{acc}}^{(d_1)}(p))^{m_{d_f}-k}, \tag{33}$$

where $p_{\text{acc}}^{(d_1)}(p)$ is the probability of acceptance for preparing the state $|\overline{H}\rangle_{d_1}$. An accepted $|\overline{H}\rangle_{d_1}$ state then grows into an encoded $|\overline{H}\rangle_{d_2}$ state since the Clifford operations are chosen to be encoded in the distance d_2 triangular color code. Since the weight-six stabilizers of the stabilizer state (and all encoded Clifford gates) are obtained from the circuit in Supplementary Fig. 7, the total number of qubits required for the stabilizer state $|S_t\rangle$ is

$$n_{S_t}(d_1, d_2) = \frac{(3d_2-1)^2}{4} - \frac{(3d_1-1)^2}{4}, \tag{34}$$

and the number of qubits for each $|\overline{H}\rangle_{d_1}$ state is

$$n_{d_1} = \frac{6{d_1}^2 - 9d_1 + 5}{2}. \tag{35}$$

Lastly, since the qubits in the implementation for preparing $|\overline{H}\rangle_f$ using the protocol of Fig. 1 in the main paper are encoded in the triangular color code with distance d_2, we require an additional

$$n_{\text{add}}(d_1, d_f) = \frac{(3d_2-1)^2(6d_f^2 - 9d_f + 5)}{8}, \tag{36}$$

qubits. Hence, the total average number of qubits $\langle n_f \rangle$ required to prepare $|\overline{H}\rangle_f$ is

$$\langle n_f(p, m_{d_f})\rangle = \frac{n_{\text{add}}(d_1, d_f) + m_{d_f}(n_{d_1} + n_{S_t}(d_1, d_2))}{P^{(n_{d_f}+1)}_{A,d_f}(p, m_{d_f})\Big(P^{(n_{d_f})}_{A,d_f}(p, m_{d_f})\Big)^{(d_f-2)}P_{A,H_f}(p)}, \tag{37}$$

where $P_{A,H_f}(p)$ is the acceptance probability for preparing $|\overline{H}\rangle_f$ with Clifford operations encoded in a distance d_2 triangular color code. For a fixed value of p, m_{d_f} is chosen to minimize Eq. (37). Note that we assume that all the qubits used to prepare the m_{d_f} $|\overline{H}\rangle_{d_1}$ states can be reused to implement the T gates at the end of the $H^{(d)}_m$ circuit. In doing so, it is assumed that the time scale required to prepare the $|\overline{H}\rangle_{d_2}$ states is less than or equal to the time scale required to implemented all the encoded operations prior to applying the T gates at the end of the $\tilde{H}^{(d)}_m$ circuit. Also, the denominator of Eq. (37) has the factor $P^{(n_{d_f}+1)}_{A,d_f}(p, m_{d_f})\Big(P^{(n_{d_f})}_{A,d_f}(p, m_{d_f})\Big)^{(d_f-2)}$ for the following reasons: In the first time step, an extra magic state is used in the $\tilde{G}^{(1\to d_f)}$ circuit (see Supplementary Fig. 6). Second, only n_{d_f} $|\overline{H}\rangle_{d_2}$ states are required when implementing the sequence of T gates (which are implemented after the $T^\dagger$ gates). The term $P^{(n_{d_f})}_{A,d_f}(p, m_{d_f})$ is taken to the power of $d_f - 2$ since the $H^{(d_f)}_m$ circuit is repeated $(d_f - 1)/2$ times (and each circuit requires the injection of n_{d_f} magic states for both the $T^\dagger$ and T gates).

If one is willing to significantly increase the time-overhead required for preparing all the magic states used in the preparation scheme of $|\overline{H}\rangle_f$, the number of qubits required to prepare $|\overline{H}\rangle_f$ can be reduced compared to the requirements given by Eq. (37). In particular, one can repeat the $|\overline{H}\rangle_{d_1}$ protocol until n_{d_f} magic states are simultaneously accepted and ready to be grown to $|\overline{H}\rangle_{d_2}$ states. Such qubits are then reused to prepare $|\overline{H}\rangle_{d_1}$ states prior to implementing the $T^\dagger$ and T gates every time the $H^{(d)}_m$ circuit is repeated. If any of the $|\overline{H}\rangle_{d_1}$ states do not pass the verification test described in Fig. 1 in the main paper, the protocol is aborted. In this case, the minimum number of qubits required to prepare $|\overline{H}\rangle_f$ is simply

$$\min(n_f(p)) = n_{\text{add}}(d_1, d_f) + (n_{d_f} + 1)(n_{d_1} + n_{S_t}(d_1, d_2)). \tag{38}$$

We now describe how to compute the space-time overhead for preparing $|\overline{H}\rangle_f$. We first need to consider the space-time overhead of preparing the m_{d_f} $|\overline{H}\rangle_{d_1}$ states, and then growing them to $|\overline{H}\rangle_{d_2}$ states. The space-time overhead for preparing a single $|\overline{H}\rangle_{d_1}$ state is obtain in a similar way to Eq. (6) in the main paper and is given by

$$S_1 = n_{d_1}(14 + \frac{(d_1 - 1)}{2}(t^{(d_1)}_{H_m} + t^{(d_1)}_{\text{EC}}), \tag{39}$$

where $t^{(d_1)}_{H_m}$ and $t^{(d_1)}_{\text{EC}}$ correspond to the number of time steps for implementing the $H^{(d_1)}_m$ and $EC^{(d_1)}$ circuits. When growing a state $|\overline{H}\rangle_{d_1}$ to $|\overline{H}\rangle_{d_2}$, the measurements of the plaquettes are repeated d_1 times, with the maximum number of time steps for each round of measurement being $t^{(d_1)}_{\text{EC}}$ (which come from measuring the stabilizers for the state $|\overline{H}\rangle_{d_1}$ using the circuits of Fig. 2 in the main paper). Therefore, the space-time overhead for growing an $|\overline{H}\rangle_{d_1}$ to $|\overline{H}\rangle_{d_2}$ state is given by

$$S^{(d_2)}_G = t^{(d_1)}_{\text{EC}} d_1(n_{S_t}(d_1, d_2) + n_{d_1}). \tag{40}$$

Since we prepare m_{d_f} such states, the space-time overhead for preparing all of the $|\overline{H}\rangle_{d_2}$ states which are injected in the $T^\dagger$ gates and the circuit $\tilde{G}^{(1\to d_f)}$ is

$$S_2 = m_{d_f}(S_1 + S^{(d_2)}_G). \tag{41}$$

The last step consists of implementing the $(d_f - 1)/2$ pairs of $\tilde{H}^{(d_f)}_m$ and $\tilde{EC}^{(d_f)}$ circuits. Each implementation of an encoded Clifford gate requires d_2 rounds of error correction, and an encoded block consists of $(3d_2 - 1)^2/4$ qubits. Furthermore, if $d_2 > 3$, the total number of time steps for one round of error correction is 16. Thus the space-time overhead for preparing $|\overline{H}\rangle_f$ with encoded Clifford gates is

$$\begin{aligned} S_{d_f} &= 16 n_{\text{add}}(d_2, d_f)(\max(14, d_2) + \\ &\frac{(d_f - 1)}{2}(\max(t^{(d_f)}_{H_m}, d_2) + \max(t^{(d_f)}_{\text{EC}}, d_2)). \end{aligned} \tag{42}$$

Note that in Eq. (42), we choose a large enough time window for the implementation of the circuits $\tilde{G}^{(1\rightarrow d_f)}$, $\tilde{H}_m^{(d_f)}$ and $\tilde{EC}^{(d_f)}$ to ensure that at least d_2 time steps occur allowing one to decode to the full d_2 color code distance. Since all logical gates in this time window are Clifford (for $H_m^{(d)}$, this is true for gates applied in between the $T^\dagger$ and T gates) and performed using lattice surgery [1–4], one can perform the appropriate Pauli frame updates to incorporate the correct decoding scheme over the full triangular color code cycle. In our numerical simulations, we pessimistically added an error at each logical Clifford gate location using the failure probabilities obtained in ref. [5] instead of using such probabilities for adding failures over a full distance d_2 triangular color code cycle. Hence the $p_L^{(d_f)}$ values reported in Supplementary Table 1 are upper bounds on the exact values that would be obtained using our scheme. Combining Eqs. (41) and (42), the total space-time overhead for the $|\overline{H}\rangle_f$ preparation scheme is given by

$$S_{\text{tot}}^{(d_f)} = \frac{S_2 + S_{d_f}}{P_{A,d_f}^{(n_{d_f}+1)}(p, m_{d_f})\Big(P_{A,d_f}^{(n_{d_f})}(p, m_{d_f})\Big)^{(d_f-2)} P_{A,H_f}(p)}. \tag{43}$$

$\lvert\overline{H}\rangle_f$	$\lvert\overline{H}\rangle_{d_1}$	p	Color code distance (d_2)	$p_L^{(d_f)}$	$\langle n_f(p, m_{d_f})\rangle$	$\min(n_f(p))$	$S_{\text{tot}}^{(d_f)}$
$d_f = 3$	$d_1 = 7$	10^{-4}	$d_2 = 11$	3.59×10^{-15}	10,917	6,288	3.91×10^6
$d_f = 5$	$d_1 = 5$	10^{-4}	$d_2 = 9$	1.10×10^{-17}	14,955	12,795	1.22×10^7
$d_f = 5$	$d_1 = 5$	2×10^{-4}	$d_2 = 11$	4.01×10^{-16}	25,265	19,320	1.88×10^7
$d_f = 5$	$d_1 = 5$	3×10^{-4}	$d_2 = 15$	6.12×10^{-17}	53,449	36,420	3.84×10^7
$d_f = 7$	$d_1 = 3$	10^{-4}	$d_2 = 7$	5.37×10^{-18}	16,262	15,600	2.30×10^7
$d_f = 7$	$d_1 = 3$	2×10^{-4}	$d_2 = 9$	5.11×10^{-17}	28,141	26,364	3.91×10^7
$d_f = 7$	$d_1 = 3$	3×10^{-4}	$d_2 = 11$	9.87×10^{-17}	43,329	39,936	5.96×10^7
$d_f = 7$	$d_1 = 3$	4×10^{-4}	$d_2 = 13$	5.74×10^{-16}	62,540	56,316	9.26×10^7
$d_f = 7$	$d_1 = 3$	5×10^{-4}	$d_2 = 15$	1.17×10^{-15}	84,200	75,504	1.156×10^8

Supplementary Table 1: Qubit and space-time overhead of various schemes using encoded Clifford gates to obtain $|\overline{H}\rangle_f$ states with logical error rates $p_L^{(d_f)} < 4\times 10^{-15}$. Here d_2 is the triangular color code distance used to encode the logical Clifford gates, d_f is distance used for the $|\overline{H}\rangle$ state preparation scheme of Fig. 1 in the main paper, d_1 is the distance of $|\overline{H}\rangle$ prior to beging grown into $|\overline{H}\rangle_{d_2}$ and p is the physical error rate. We provide both the average number of qubits (given by Eq. (37)) and also the minimum number of qubits (see Eq. (38)) for preparing $|\overline{H}\rangle_f$. The space-time overhead is given by Eq. (43).

In Supplementary Table 1 we provide the average number of qubits, minimum number of qubits and space-time overhead required to prepare $|\overline{H}\rangle_f$ states with logical failure rates $p_L^{(d_f)} < 4 \times 10^{-15}$. To obtain such results, we assume that each Clifford gate encoded in the triangular color code fails according to the logical error rate polynomials obtained in ref. [5] (which we call $p_{LC}^{(d_2)}(p)$). Hence, when preparing the stabilizer state $|S_t\rangle$ and for all encoded Clifford operations, the ancilla qubit layout for the weight-six checks are chosen as in Supplementary Fig. 7 (note that the weight-four checks remain unchanged). Further, the distance d_1 is chosen to be the smallest d_1 which ensures that $|\overline{H}\rangle_{d_1}$ has a lower logical error rate than $p_{LC}^{(d_2)}(p)$. Lastly, due to the low failure rates of the encoded components, to obtain $p_L^{(d_f)}$ we repeat the simulation described in the Methods section of the main paper for physical values of $p > 10^{-3}$, and extrapolate the best fit curves to the regime where $p \in [10^{-4}, 5 \times 10^{-4}]$.

The numerical values obtained in Supplementary Table 1 shows that the least costly scheme to prepare the state $|\overline{H}\rangle_f$ with $p_L^{(d_f)} < 4\times 10^{-15}$ when $p = 10^{-4}$ is to first prepare the states $|\overline{H}\rangle_{d_1}$ with $d_1 = 7$, and to grow these states to encoded $d_2 = 11$ states. Using distance $d_2 = 11$ encoded stabilizer operations, the final magic state $|\overline{H}\rangle_f$ is prepared using the distance $d_f = 3$ scheme of Fig. 1 in the main paper. On average, the amount of qubits required to prepare such a state is 10,917 and the space-time overhead is 3.91×10^6. If the time cost for preparing the $|\overline{H}\rangle_{d_1}$ states is of a lesser concern, the minimum number of qubits required to prepare $|\overline{H}\rangle_f$ with $p_L^{(d_f)} < 4 \times 10^{-15}$ is 6,288. To compare with other schemes, in ref. [6], a magic state with a logical error failure rate of 2.4×10^{-15} required a minimum of 16,400 qubits.

To obtain a state $|\overline{H}\rangle_f$ with $p_L^{(d_f)} \approx 10^{-15}$ when $p = 10^{-3}$ using a small amount of resources requires encoded stabilizer operations with much lower logical failure rates than what is achieved with the triangular color code family. One viable option is to use stabilizer operations encoded in the surface code due to the low error rates that can be achieved when $p = 10^{-3}$ [7]. However, in such a setting, after the states $|\overline{H}\rangle_{d_2}$ have been prepared, they must be teleported to the surface code before they can be injected in the circuit of Fig. 5a in the main paper and in the circuit implementing $\tilde{G}^{(1\rightarrow d_f)}$. In particular, one can convert the color code encoded state to the surface code using lattice surgery techniques as was done in Ref. [8]. In Supplementary Table 2 we provide estimates of the qubit overhead for preparing $|\overline{H}\rangle_f$ when the stabilizer operations are encoded in the surface code. The cost of first encoding the states $|\overline{H}\rangle_{d_2}$ in the color code and then using extra qubits to convert such states into the surface code is taken into account. However, we assume that the quality of the encoded $|\overline{H}\rangle_{d_2}$ states does not change when performing lattice surgery. Although such an omission is optimistic, we verified numerically that when only the T and $T^\dagger$ gate locations are allowed to fail, the protocol of Fig. 1 in the main paper produces $|\overline{H}\rangle_f$ states with logical error rates two to four orders of magnitude (depending on the value of p) less than when all stabilizer operations fail according to the noise model described in the Methods section in the main paper. As such, the simulation provides evidence that the logical error rates obtained in Supplementary Table 2 are good estimates of the error rates that would be obtained when considering errors introduced when performing lattice surgery to obtain surface code encoded $|\overline{H}\rangle_{d_2}$ states.

$\lvert\overline{H}\rangle_f$	$\lvert\overline{H}\rangle_{d_1}$	p	Surface code distance (d_2)	$p_L^{(d_f)}$	$\langle n_f(p, m_{d_f})\rangle$	$\min(n_f(p))$
$d_f = 7$	$d_1 = 3$	10^{-4}	$d_2 = 5$	5.07×10^{-17}	10,025	9,506
$d_f = 7$	$d_1 = 3$	10^{-3}	$d_2 = 11$	8.11×10^{-20}	60,886	47,324

Supplementary Table 2: Qubit overhead of schemes for obtaining an encoded $|\overline{H}\rangle_f$ as in Fig. 1 in the main paper, but with logical stabilizer operations encoded in a distance d_2 surface code. Note that the states $|\overline{H}\rangle_{d_2}$ are first encoded in the color code, and lattice surgery is performed to obtain an $|\overline{H}\rangle_{d_2}$ state encoded in the surface code as in Ref. [8].

Instead of performing lattice surgery to convert a color code encoded $|\overline{H}\rangle_{d_2}$ state to one encoded in the surface code, another option would be to initially prepare an encoded $|\overline{H}\rangle_{d_2}$ state in a small distance surface code using some other method, such as a magic state distillation protocol. The $|\overline{H}\rangle_{d_2}$ states would then be injected in the T gate circuits of Fig. 5a in the main paper in addition to the $\tilde{G}^{(1\to d_f)}$ circuit in order to prepare an $|\overline{H}\rangle_f$ state using the methods presented in Fig. 1 in the main paper. To obtain comparable logical failure rates to the ones shown in Supplementary Table 1 (say $p_L^{(d_f)} \leq 10^{-15}$) at $p = 10^{-3}$, the surface code distance d_2 would need to be $d_2 = 15$ if the $d_f = 3$ scheme was chosen, $d_2 = 13$ if the $d_f = 5$ scheme was chosen and $d_2 = 11$ if the $d_f = 7$ scheme were chosen. Note that the logical error rate of the surface code is given by 10^{-9} for $d_2 = 15$, 10^{-8} for $d_2 = 13$, and 10^{-7} for $d_2 = 11$ [7]. In contrast, $d_2 \geq 27$ would be required if conventional non fault-tolerant magic state distillation schemes are used, since in this case the stabilizer operations should have a logical error rate as low as 10^{-15}. A careful analysis of the overhead would require choosing the appropriate magic state distillation protocol (or some other scheme which uses fault-tolerant circuits to prepare encoded magic states) and therefore such an analysis is left for future work.

One could also directly prepare an encoded $|\overline{H}\rangle_{d_2}$ state in a distance d_2 surface code using the non-fault-tolerant state injection methods of ref. [9]. Such states would then be injected in the scheme for preparing $|\overline{H}\rangle_f$ (see Supplementary Fig. 6) with encoded stabilizer operations in a distance d_2 surface code. In this case, the injected $|\overline{H}\rangle_{d_2}$ states would have much higher failure rates compared to the encoded stabilizer operations. In such a setting, extending our scheme to $d_f \geq 9$ could potentially be very beneficial. However, to avoid preparing a state $|\overline{H}\rangle_f$ with $d_f > 7$, one could consider a two level approach. As a first step, one could inject $|\overline{H}\rangle_{d_2}$ states to first prepare an $|\overline{H}\rangle_f$ state with $d_f \leq 5$. Afterwords, the obtained $|\overline{H}\rangle$ could be further injected to prepare a new $|\overline{H}\rangle_f$ state with $d_f \geq 5$.

Note also that the underlying codes that are used for our work belong to the triangular color code family. One avenue of exploration would be to consider the 4.8.8 color code family (see for instance Refs. [10, 11]) for potentially better performance. In addition, the color codes used to encode the Clifford operations required two and three ancillas for the weight-four and weight-six stabilizers respectively. Using similar edge weight renormalization schemes to those described in Ref. [5], one could use fewer ancillas for measuring each stabilizer while maintaining the full effective code distance of the Lift decoder. Due to the smaller number of fault locations and reduced ancilla requirements, such an implementation could potentially significantly reduce the overhead for preparing encoded $|H\rangle$ states.

When considering the implementation of our scheme with encoded stabilizer operations using the surface code, the $d_f = 7$ version of our scheme was optimal for both $p = 10^{-4}$ and $p = 10^{-3}$. A clear direction of future work would be to find a v-flag circuit (with $v \geq 4$) allowing a fault-tolerant implementation of a $d_f \geq 9$ scheme. Such a scheme could potentially further reduce the overhead for preparing $|H\rangle$ states with very low error rates.

The schemes considered in this work to prepare $|H\rangle$ states are error detection schemes. In particular, for $p = 10^{-3}$ and $d_f > 3$, the acceptance probability for preparing an $|H\rangle$ state is very low (for instance, only 12% when $d_f = 5$). One way to improve the acceptance probability could be to use qubits encoded in a bosonic code [12] (such as a GKP code [13]) and concatenate such qubits with the color code (the GKP code concatenated with the surface code was considered in Refs. [14–16] for quantum memories). By using bosonic qubits, repeated rounds of error correction at the bosonic level prior to measuring the logical Hadamard operator and stabilizers of the color code could be performed to reduce some of the errors afflicting the data and ancilla qubits. Another possibility would be to develop an error correction scheme for preparing an $|H\rangle$ state which applies directly to the color code family. Such a scheme would have higher logical error rates compared to an error detection scheme, and the scheduling of the controlled-Hadamard gates would have to be considered more carefully. However, since an error correction scheme would not require any post selection, there could be an interval of physical error rates where it achieved better performance compared to the error detection scheme considered in this work.

[1] C. Horsman, A. G. Fowler, S. Devitt, and R. V. Meter, "Surface code quantum computing by lattice surgery," New J. Phys. **14**, 123011 (2012).
[2] A. J. Landahl and C. Ryan-Anderson, "Quantum computing by color-code lattice surgery," arXiv e-prints , arXiv:1407.5103 (2014), arXiv:1407.5103 [quant-ph] .
[3] D. Litinski and F. v. Oppen, "Lattice Surgery with a Twist: Simplifying Clifford Gates of Surface Codes," Quantum **2**, 62 (2018).
[4] A. G. Fowler and C. Gidney, "Low overhead quantum computation using lattice surgery," arXiv:1808.06709 (2018).
[5] C. Chamberland, A. Kubica, T. J. Yoder, and G. Zhu, "Triangular color codes on trivalent graphs with flag qubits," New J. Phys. **22**, 023019 (2020).
[6] D. Litinski, "Magic State Distillation: Not as Costly as You Think," Quantum **3**, 205 (2019).
[7] A. G. Fowler, A. C. Whiteside, A. L. McInnes, and A. Rabbani, "Topological code autotune," Phys. Rev. X **2**, 041003 (2012).
[8] H. P. Nautrup, N. Friis, and H. J. Briegel, "Fault-tolerant interface between quantum memories and quantum processors," Nat. Commun. **8**, 1321 (2017).
[9] Y. Li, "A magic state's fidelity can be superior to the operations that created it," New J. Phys. **17**, 023037 (2015).
[10] A. J. Landahl, J. T. Anderson, and P. R. Rice, "Fault-tolerant quantum computing with color codes," arXiv:1108.5738 (2011).
[11] M. S. Kesselring, F. Pastawski, J. Eisert, and B. J. Brown, "The boundaries and twist defects of the color code and their applications to topological quantum computation," Quantum **2**, 101 (2018).
[12] V. V. Albert, K. Noh, K. Duivenvoorden, D. J. Young, R. T. Brierley, P. Reinhold, C. Vuillot, L. Li, C. Shen, S. M. Girvin, B. M. Terhal, and L. Jiang, "Performance and structure of single-mode bosonic codes," Phys. Rev. A **97**, 032346 (2018).
[13] D. Gottesman, A. Kitaev, and J. Preskill, "Encoding a qubit in an oscillator," Phys. Rev. A **64**, 012310 (2001).
[14] K. Fukui, A. Tomita, A. Okamoto, and K. Fujii, "High-threshold fault-tolerant quantum computation with analog quantum error correction," Phys. Rev. X **8**, 021054 (2018).
[15] C. Vuillot, H. Asasi, Y. Wang, L. P. Pryadko, and B. M. Terhal, "Quantum error correction with the toric gottesman-kitaev-preskill code," Phys. Rev. A **99**, 032344 (2019).
[16] K. Noh and C. Chamberland, "Fault-tolerant bosonic quantum error correction with the surface–gottesman-kitaev-preskill code," Phys. Rev. A **101**, 012316 (2020).